

## Simple solar panels/battery modeling for spacecraft power distribution systems

Ángel Porras-Hermoso, Borja Cobo-Lopez, Javier Cubas, Santiago Pindado\*

Instituto Universitario de Microgravedad "Ignacio Da Riva" (IDR/UPM), ETSI Aeronáutica y del Espacio, Universidad Politécnica de Madrid, Pza. del Cardenal Cisneros 3, Madrid, 28040, Spain

### ARTICLE INFO

**Keywords:**

Solar array  
 Battery  
 DC-DC converter  
 Satellite electric power system  
 DET  
 MPPT

### ABSTRACT

To progress towards as quick as possible feasible pre-design of space missions, spacecraft early design today is organized gathering together experts from different spacecraft subsystems that share information (and results). This Concurrent Design (CD) approach needs accurate but quick solutions from all subsystems involved in each phase of that mission early design. At IDR/UPM Institute researchers have been working in simplified models for the spacecraft power distribution subsystem. In the present paper three models, for solar panels, the battery and DC-DC converters are described and tested with experimental data. The models were designed to be coupled within the simulation of a spacecraft mission. The model regarding the solar panels is focused on accurately estimate the power production from the panels, whereas the model of the batteries is based on the discharged energy rate as the main/control parameter instead of the discharged/charged ampere-hour rate. Finally, the solar-panels/battery coupled design is described in this paper, the UPMSat-2 mission being used as case study.

### 1. Introduction

As a result of the scientific, technical and academic work at the IDR/UPM Institute, many contributions on space systems have been produced in the last years. Together with results from the well-established research/technical lines of work on thermal and mechanical engineering [1–6], some quite relevant works on power systems (focused on solar cells/panels) have been published [7–14]. Additionally, the work carried out in relation to the UPMSat-2 power system since 2014 has allowed us to carry out a quite intensive research on Li-ion battery modeling, specially related to battery maintenance and testing, and cells balancing (see Fig. 1).

In the present work, a solar-panel-battery coupled analysis is described, the case study being composed by experimental results and data from the UPMSat-2 mission [12,15,16]. In relation to the solar panels performance, the analytical methodologies developed at the IDR/UPM Institute to study solar cells/panels are used to model the performance of the UPMSat-2 solar panels during the mission. The model is tuned with the experimental data from one of the Selex Galileo SPVS-X5 modules that form each one of the UPMSat-2 lateral panels.

With regard to the batteries performance, the model initially proposed as a result of the first fittings to experimental results [17] is

analyzed in the present work. The effect of the different terms of the equations on the model's accuracy in relation to the experimental data is thoroughly studied, in order to quantify their relative importance in the model. Besides, the effect of the discharging/charging current on the different coefficients is also studied.

The aim of this work is to study the coupled performance of a simple spacecraft power distribution subsystem, considering its different sub parts (solar panels, battery), and to test the proposed models in order to have a simple but accurate methodology. The solutions included in this work are intended to be:

- Easily integrated in space mission simulations carried out in a Concurrent Design Facility (CDF), in order to reduce the time required to derive an early design of the studied mission [18–22].
- Easily programmed in more complex coupled simulations that would require harmonization with thermal effects. In this latter case, it should be underlined the importance of simplified and easy-to-work-with equations for modeling the performance of electric systems, as it has been recently revealed by the research carried out at the IDR/UPM Institute in relation to thermo-electric coupled analysis of the UPMSat-2 [23].

\* Corresponding author.

E-mail address: [santiago.pindado@upm.es](mailto:santiago.pindado@upm.es) (S. Pindado).

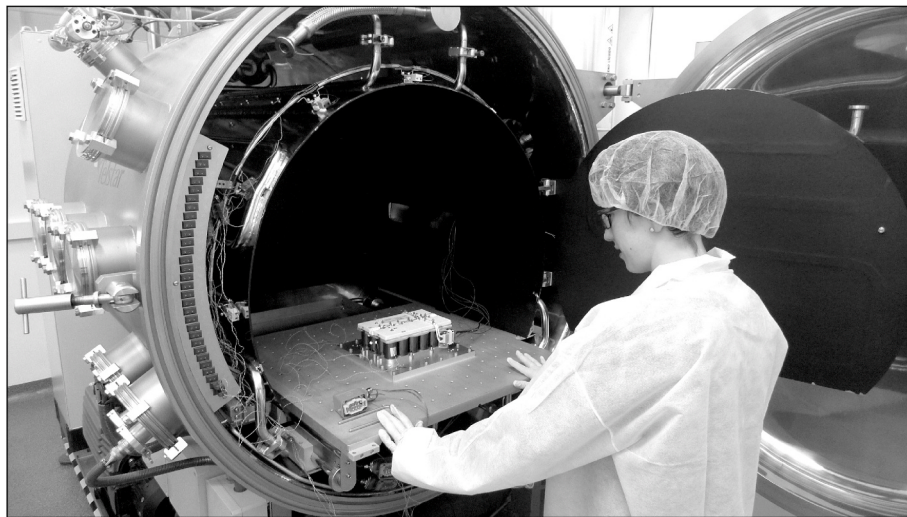


**Fig. 1.** Battery of the UPMSat-2 being tested at the thermal vacuum facility of the IDR/UPM Institute.

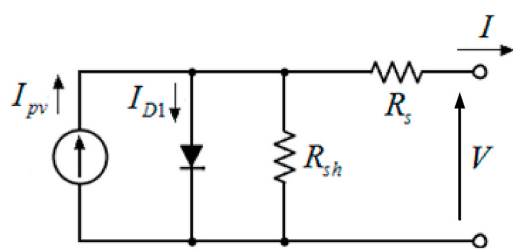


**Fig. 2.** 1-D/2-R equivalent circuit model for analyzing solar cell/panel performance [7].

The more relevant contributions of this work are:

- The definition of models for different parts of spacecraft power distribution subsystem.
- The results of the case study carried out in relation to the UPMSat-2 mission (launched on September the 2nd 2020 from the *Centre Spatial Guyanais* –French Guiana, France– with VV16 VEGA rocket), which indicate a better performance of the Direct Energy Transfer (DET) architecture in relation to a Maximum Power Point Tracking (MPPT) design.

This paper is organized as follows. In Section 2 the solar panel models are described, together with the DC/DC converters modeling. The battery modeling is included in Section 3. The simulation of the UPMSat-2 power subsystem is carried out in Section 4, as case study. Finally, the conclusions of this work are summarized in Section 5.

## 2. Spacecraft solar panels simulation

Probably, the most common way to study the performances of a solar panel is by using the equivalent electric circuit formed by an ideal current source, a diode, a shunt resistor and a series resistor. This is the commonly known as the 1-Diode and 2-Resistor (1-D/2-R) equivalent circuit model (see Fig. 2). The equation of that circuit is the following:

$$I = I_{pv} - I_{D1} - \frac{V + IR_s}{R_{sh}} = I_{pv} - I_0 \left[ \exp\left(\frac{V + IR_s}{naV_T}\right) - 1 \right] - \frac{V + IR_s}{R_{sh}}, \quad (1)$$

where  $I_{pv}$  is the photocurrent,  $I_0$  is the reverse saturation current of the diode,  $a$  is the ideality factor,  $n$  is the number of series connected cells of the solar panel,  $R_{sh}$  is shunt resistor,  $R_s$  is the series resistor,  $V_T = \kappa T/q$  is

the thermal voltage,  $\kappa$  being the Boltzmann constant,  $T$  the solar panel cells temperature, and  $q$  the electron charge.

In order to work with the equation above, it is firstly required to extract the five parameters,  $I_{pv}$ ,  $I_0$ ,  $a$ ,  $R_s$  and  $R_{sh}$ , that configure the proper fit of the model to the real working conditions of the solar panel (that is, its output current-voltage or  $I$ - $V$  curve). This is not an easy task that requires, in principle, expertise on numerical calculation for fitting equation (1) to the  $I$ - $V$  curve of the panel. A different strategy is to use the current and voltage levels data from the characteristic points of the aforementioned curve, short circuit, maximum power, and open circuit ( $I_{sc}$ ,  $I_{mp}$ ,  $V_{mp}$ ,  $V_{oc}$ ). There are several works on the different techniques to extract the parameters of the 1-D/2-R equivalent circuit models [24–31]. At the IDR/UPM Institute some simple methodologies for analyzing solar panel performances in space environment have been developed [32,33]. The reason for developing these simple techniques lies on the need of coupling the electric calculations with simulations of the thermal behavior of a spacecraft (or its attitude control behavior), and the need of quick solutions within Concurrent Design (CD) of space missions.

Equation (1) can be solved firstly by selecting a proper value for the ideality factor (one of the last researches at the IDR/UPM seems to indicate that  $a = 1$  can be selected for all photovoltaic technologies [35]), and then using the following equations for getting the series resistor as a function of the characteristic points:

$$R_s = A(W_{-1}(B \exp(C)) - (D + C)), \quad (2)$$

$$A = \frac{naV_T}{I_{mp}}, \quad (3)$$

$$B = -\frac{V_{mp}(2I_{mp} - I_{sc})}{V_{mp}I_{sc} + V_{oc}(I_{mp} - I_{sc})}, \quad (4)$$

$$C = -\frac{2V_{mp} - V_{oc}}{naV_T} + \frac{V_{mp}I_{sc} - V_{oc}I_{mp}}{V_{mp}I_{sc} + V_{oc}(I_{mp} - I_{sc})}, \quad (5)$$

$$D = \frac{V_{mp} - V_{oc}}{naV_T}. \quad (6)$$

In the above equation (2),  $W_{-1}$  is the negative branch of the Lambert W-function. Once the series resistor is calculated, it is possible to obtain the other three parameters with the following equations:

$$R_{sh} = \frac{(V_{mp} - I_{mp}R_s)(V_{mp} - R_s(I_{sc} - I_{mp}) - naV_T)}{(V_{mp} - I_{mp}R_s)(I_{sc} - I_{mp}) - naV_T I_{mp}}, \quad (7)$$

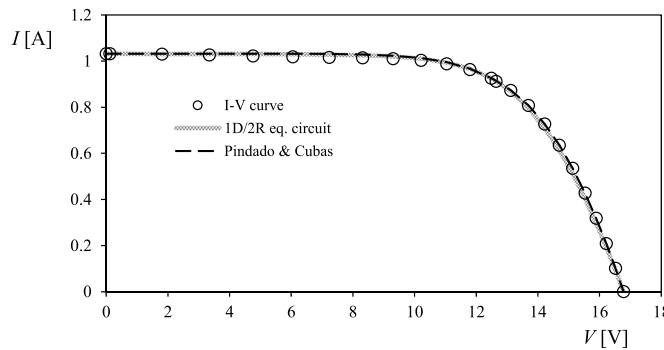


**Fig. 3.** Measured  $I$ - $V$  curve from a Photowatt PWP 201 solar panel [34]. The fittings of the 1-D/2-R equivalent circuit model (equation (1)), and the Pindado & Cubas model (equation (11)) to these data have been also included in the graph.

$$I_{pv} = \frac{R_{sh} + R_s}{R_{sh}} I_{sc}, \quad (8)$$

and:

$$I_0 = \frac{(R_{sh} + R_s) I_{sc} - V_{oc}}{R_{sh} \exp\left(\frac{V_{oc}}{naV_T}\right)}. \quad (9)$$

The above equations define perfectly the performance of a solar panel in relation to the characteristic points of the  $I$ - $V$  (known for a certain irradiance level,  $G$ , and a certain temperature of the solar cells,  $T$ ). The variation of the characteristic points with regard to these last two parameters have been studied by many researchers, a quite large number of mathematical expressions having been developed to ease the calculations [36–41]. Finally, any researcher has to deal with a last difficulty: equation (1) is an implicit mathematical expression. Therefore, an iterative process needs to be carried out to derive the output current in relation to a certain output voltage level. Fortunately, the Lambert W-function (more precisely, the positive branch,  $W_0$ , of the Lambert-W function), can be used for solving this problem [42]:

$$I = \frac{R_{sh}(I_{pv} + I_0) - V}{R_{sh} + R_s} - \frac{naV_T}{R_s} W_0\left(\frac{R_{sh}R_s I_0}{naV_T(R_{sh} + R_s)} \exp\left(\frac{R_{sh}R_s(I_{pv} + I_0) + R_{sh}V}{naV_T(R_{sh} + R_s)}\right)\right), \quad (10)$$

specially if simplified solutions of the Lambert W-function are taken into account [32,33].

Additionally, an explicit equation for modeling solar cell/panel behavior was developed at the IDR/UPM [13]:

$$I = \begin{cases} I_{sc} \left(1 - \left(1 - \frac{I_{mp}}{I_{sc}}\right) \left(\frac{V}{V_{mp}}\right)^{\frac{I_{mp}}{I_{sc} - I_{mp}}}\right) & ; V \leq V_{mp} \\ I_{mp} \left(\frac{V_{mp}}{V}\right) \left(1 - \left(\frac{V - V_{mp}}{V_{oc} - V_{mp}}\right)^{\xi}\right) & ; V \geq V_{mp} \end{cases}, \quad (11)$$

where:

$$\xi = \left(\frac{I_{sc}}{I_{mp}}\right) \left(\frac{I_{sc}}{I_{sc} - I_{mp}}\right) \left(\frac{V_{oc} - V_{mp}}{V_{oc}}\right) \quad (12)$$

In Fig. 3, the results of these fittings to the experimental  $I$ - $V$  curve from a Selex Galileo SPVS X5 solar module area plotted. It can be observed that both models (equations (1) and (11)) fit quite well the experimental results. It should be also pointed out that variations of the irradiance,  $G$ , and temperature,  $T$ , should be taken into account in the aforementioned models. The following expressions can be used in this regard:

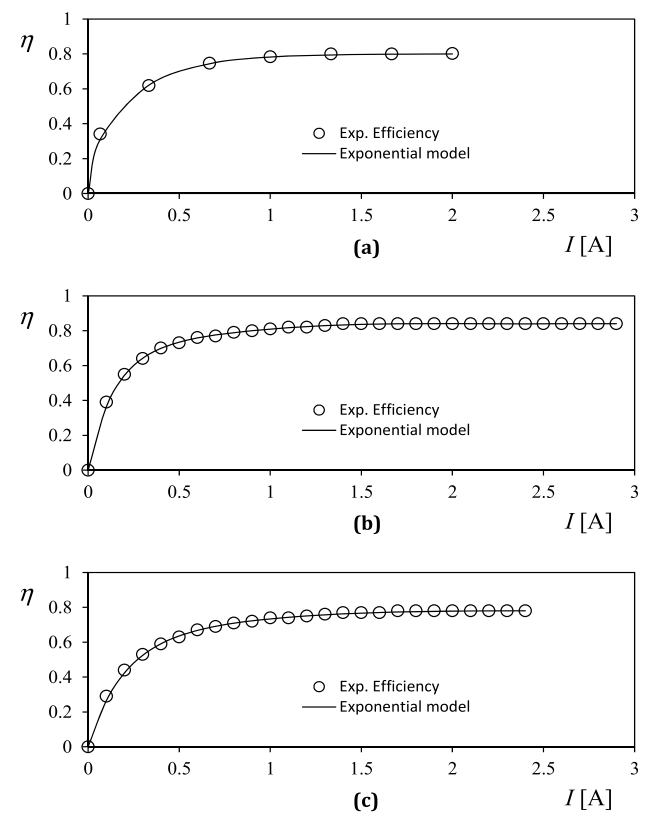


**Fig. 4.** Efficiencies,  $\eta$ , of the (a) Bus-Voltage to  $\pm 15$  V, (b)  $+15$  V to  $+5$  V, and (c)  $+15$  V to  $+3.3$  V DC/DC converters of the UPMsat-2 in relation to the output current,  $I$ . The experimental data and the exponential model fitted (see also equation (17) and Table 1), are included in the graphs.

$$I_{sc} = \frac{G}{G_0} [I_{sc0} + \alpha_{isc}(T - T_0)]. \quad (13)$$

$$I_{mp} = \frac{G}{G_0} [I_{mp0} + \alpha_{imp}(T - T_0)]. \quad (14)$$

$$V_{mp} = V_{mp0} + aV_T \ln \frac{G}{G_0} + \alpha_{vmp}(T - T_0). \quad (15)$$

$$V_{oc} = V_{oc0} + aV_T \ln \frac{G}{G_0} + \alpha_{voc}(T - T_0). \quad (16)$$

where  $\alpha_{isc}$ ,  $\alpha_{imp}$ ,  $\alpha_{vmp}$  and  $\alpha_{voc}$  are coefficients that define the variation of the corresponding parameter with the temperature,  $T$ . The subscript “0” indicates values at Standard Test Conditions (STC). This information is normally given by the solar cells’ manufacturer.

### 2.1. The control of the maximum power point (MPP). Performance of DC/DC converters

The way to connect the solar panels to the battery is matter of a great concern in small satellites [43,44]. In general, two opposite possibilities are available:

- Direct Energy Transfer (DET), which consist in a direct connection of the solar panel to the battery (or to a bus where the battery is directly connected to). This is a robust system. However, the operation point of the solar panels (that is, the point of the  $I$ - $V$  curve in which the solar panel is working), depends both on the battery voltage and the solar panels temperature [45]. As a result, the solar panel will not be

**Table 1**

Maximum efficiencies,  $\eta_{\max}$ , and mathematical expressions,  $f(I)$ , to fit the exponential model from equation (17) to the experimental data (see Fig. 4).

DC/DC converter	$\eta_{\max}$	$f(I)$
Bus-Voltage to $\pm 15$ V	0.80	$-(11.58I^2 + 2.837I)^{1/2}$
+15 V to +5 V	0.84	$-2.3472I^3 + 5.212I^2 - 6.1638I$
+15 V to +3.3 V	0.78	$-0.8942I^3 + 2.4503I^2 - 4.38I$

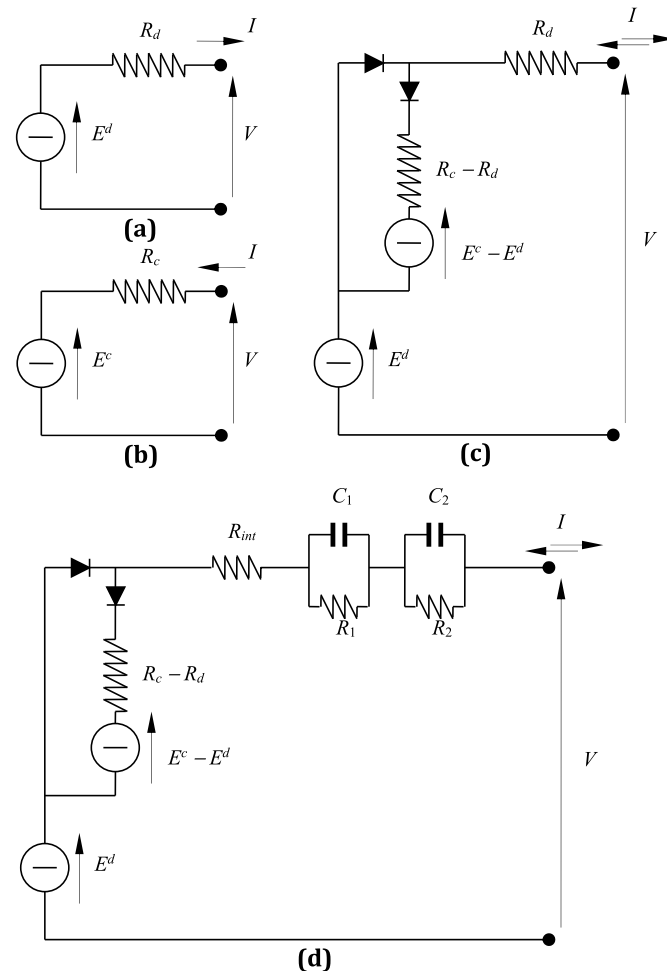


**Fig. 5.** (a) Equivalent circuit model for a li-ion battery during discharging process. (b) Equivalent circuit model for a li-ion battery during charging process. (c) Li-ion battery model for both static (that is, at constant current rate) charging and discharging processes. (d) Complete Li-ion battery model proposed, for static and dynamic (at not constant current rate) performance.

working at the Maximum Power Point (MPP) [43]. Obviously, this direct connection is secured with diodes to avoid reverse currents towards the solar panels [43].

- Maximum Power Point Tracking (MPPT), this configuration includes a system to force the solar panels output voltage to the MPP. This is a more complex system that would require a more thorough analysis to avoid failure modes of the power sub-system. The main advantage is that the solar panels are always supplying the maximum power [44], and therefore less irradiated power is wasted in heating them. However, the MPPT is a DC/DC voltage converter that has some power consumption that needs to be taken into account [43,45,46].

In the UPMSat-2 power sub-system, three DC/DC voltage converters are present: Bus-Voltage to  $\pm 15$  V, +15 V to +5 V, and +15 V to +3.3 V,

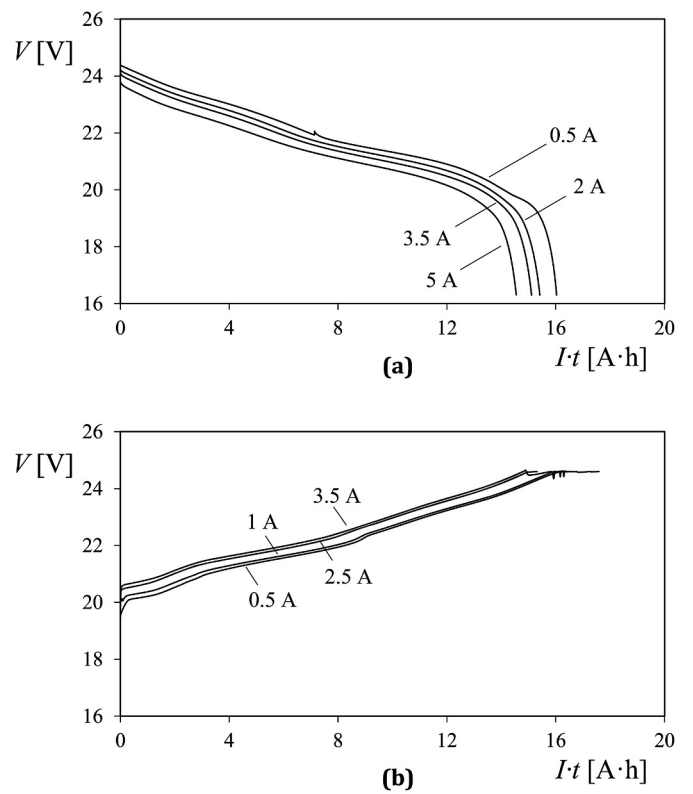


**Fig. 6.** Discharging (a) and charging (b) processes performed to the Li-ion battery tested.

their efficiencies,  $\eta$ , being dependent on the output current,  $I$  (see Fig. 4). The equation that defines the performance of these DC/DC voltage converters is (see also Table 1):

$$\eta = \eta_{\max} (1 - \exp(f(I))). \quad (17)$$

### 3. Li-ion battery simulation

#### 3.1. Battery modeling

The Li-ion battery model described in this section depends mainly on the discharged energy rate,  $\phi$ . This variable represents the amount of energy discharged in relation to the full-charge state of the battery. The discharged energy rate,  $\phi$ , is then defined for discharging processes as:

$$\phi = \phi_0 + \int_{t_0}^t E^d I dt = \phi_0 + \int_{t_0}^t (VI + R_d I^2) dt, \quad (18)$$

whereas for charging processes is defined as:

$$\phi = \phi_0 - \int_{t_0}^t E^c I dt = \phi_0 - \int_{t_0}^t (VI - R_c I^2) dt. \quad (19)$$

In the above equations  $E^d$  and  $E^c$  are the internal voltage level of the battery during discharging and charging respectively (see Fig. 5),  $I$  is the output/input current,  $R_d$  and  $R_c$  are the internal resistor during discharging and charging procedures, and  $\phi_0$  is the battery level of discharge at instant  $t_0$ . The output voltage,  $V$ , from each process is expressed as:

$$V(\phi, I) = E^d(\phi, E_0^d, E_1^d, E_2^d \dots) - R_d I, \quad (20)$$

$$V(\phi, I) = E^c(\phi, E_0^c, E_1^c, E_2^c \dots) + R_c I, \quad (21)$$

the internal battery voltages being expressed in relation to the discharged energy,  $\phi$ , and a group of constants/parameters to be extracted,

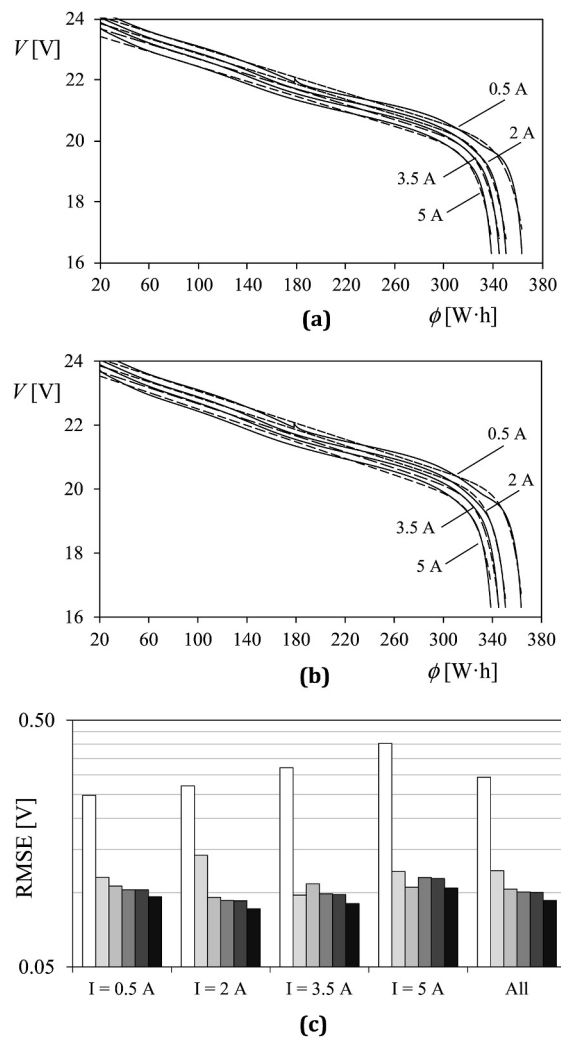


**Fig. 7.** Discharging curves of the tested battery: (a) fittings of equation (23) to each one of the curves (see also the coefficients corresponding to each fitting in Table 2), and (b) fittings of equation (28) to all curves (see Table 3). (c) RMSE of the analyzed battery discharging models (results from equations (23)–(28) fitted to all currents data –see Table 3–).

that might be also dependent on the current  $I$ . The model of the battery proposed includes hysteresis performance and it is represented by the circuit shown in Fig. 5. The non-static or dynamic performance is normally taken into account by adding two pairs of RC parallel elements connected in series to the static models [47–49], also depicted Fig. 5. In this case, obviously:

$$R_d = R_{int} + R_1 + R_2. \quad (22)$$

The results from different discharging/charging processes performed to a 17.2 A h Li-ion battery composed of Samsung INR 18650-25R cells [50] were used. The discharging processes were carried out at  $I = 0.5, 2, 3.5$  and 5 A current rates, whereas the charging processes were carried

out at  $I = 0.5, 1, 2.5$  and 3.5 A current rates (see Fig. 6). The hardware included a Mayuno M9812 DC Electronic Load controlled by Mayuno M9711 software, and an ISO-TECH IPS3303 Bench Power Supply. This battery is very similar in terms of capacity and technology (Li-ion) to the UPMSat-2, manufactured by Saft Batteries and based on VES16 cells.

### 3.2. Discharging process

The initial equation of the proposed model for the battery internal voltage discharging process is the following:

$$V(\phi, I) = E_0^d + E_1^d \phi + E_2^d \exp(E_3^d \phi) - R_d I. \quad (23)$$

The above equation was proposed taking into account the shape of the discharging processes (Fig. 6), that suggest a linear model in relation to the discharged energy,  $\phi$ , up to the sudden arrival of a very quick discharge, represented by the exponential term of the equation. Besides, the effect of the series resistor on the battery performance has been previously stated [49,51–53].

The results of the model fittings to the experimental results, once translated from the  $V$ - $I$ - $t$  curves (Fig. 6) to the  $V$ - $\phi$  curves (Fig. 7) are included in Table 2. In this table, the coefficients corresponding to the above equation, fitted individually to each one of the discharging curves have been included. The Root Mean Squared Error (RMSE) of these curves in relation to the measured data has been also included in Table 2.

The extracted coefficients (Table 2), made non-dimensional with their own values at  $I = 0.5$  A,  $e_0^d = E_0^d/E_0^d|_{I=0.5}$ ,  $e_1^d = E_1^d/E_1^d|_{I=0.5}$ ,  $e_2^d = E_2^d/E_2^d|_{I=0.5}$ ,  $e_3^d = E_3^d/E_3^d|_{I=0.5}$ , and  $r = R_d/R_d|_{I=0.5}$ , are plotted in Fig. 8 (open circles) in relation to the discharging current,  $I$ . The calculations of the discharged energy rate,  $\phi$ , with equation (18), were carried out taking into account a constant value of the internal resistor  $R_d = 0.1472 \Omega$ , extracted from an initial estimation. This is a reasonable assumption as the value of this parameter can be quite well estimated from the discharging curves (Fig. 7).

The coefficients  $E_0^d$  and  $E_2^d$  show a linear relation with the current, whereas the coefficient  $E_1^d$  shows the larger variations, suggesting a second order polynomial variation. The coefficient  $E_1^d$  does not seem to follow a linear pattern, the use of an exponential relationship with the discharged energy being suggested. Going back to coefficient  $E_0^d$ , it might be premature to suppose a linear relationship with the current, as this would suggest that the slope of this relationship is a resistor (effect which is taken into account with the variable  $R$ ). Finally, this resistor effect seems to follow a linear pattern in relation to the discharging current.

In order to further analyze the effect of the current on the coefficients from equation (23), a step-by-step approach was followed. Firstly, coefficient  $E_0^d$  was given a fixed value (as said, a linear relationship with the current would indicate a resistor effect), and then the equation was fitted to all discharging curves (see in Table 3 the coefficients resulting from this fitting). The non-dimensional results have been also included in the graphs from Fig. 8 (open squares). The tendencies shown by the coefficients in relation to the current are the same as shown by the previous approximation (open circles), with the exception of  $E_0^d$  (obviously), and  $E_1^d$ . In case of the latter, the pattern of the coefficients changed, the slope changing from being negative to positive. Therefore,

**Table 2**

Coefficients of equation (23) fitted to each one of the discharging curves,  $I = 0.5, 2, 3.5$ , and 5 A (see Fig. 7).

Coefficient/RMSE	$I = 0.5$ A	$I = 2$ A	$I = 3.5$ A	$I = 5$ A
$E_0^d$ [V]	24.336	24.223	24.1687	24.080
$E_1^d$ [V·W <sup>-1</sup> h <sup>-1</sup> ]	$-1.2531 \cdot 10^{-2}$	$-1.2443 \cdot 10^{-2}$	$-1.2431 \cdot 10^{-2}$	$-1.2297 \cdot 10^{-2}$
$E_2^d$ [V]	$-3.3834 \cdot 10^{-13}$	$-3.4087 \cdot 10^{-13}$	$-1.8816 \cdot 10^{-13}$	$-1.3033 \cdot 10^{-13}$
$E_3^d$ [W <sup>-1</sup> h <sup>-1</sup> ]	$8.1707 \cdot 10^{-2}$	$8.4973 \cdot 10^{-2}$	$8.7951 \cdot 10^{-2}$	$9.0526 \cdot 10^{-2}$
$R_d$ [ $\Omega$ ]	$1.7280 \cdot 10^{-2}$	$6.0977 \cdot 10^{-2}$	$6.8908 \cdot 10^{-2}$	$8.1734 \cdot 10^{-2}$
RMSE [V]	$1.029 \cdot 10^{-1}$	$8.953 \cdot 10^{-2}$	$8.670 \cdot 10^{-2}$	$8.729 \cdot 10^{-2}$

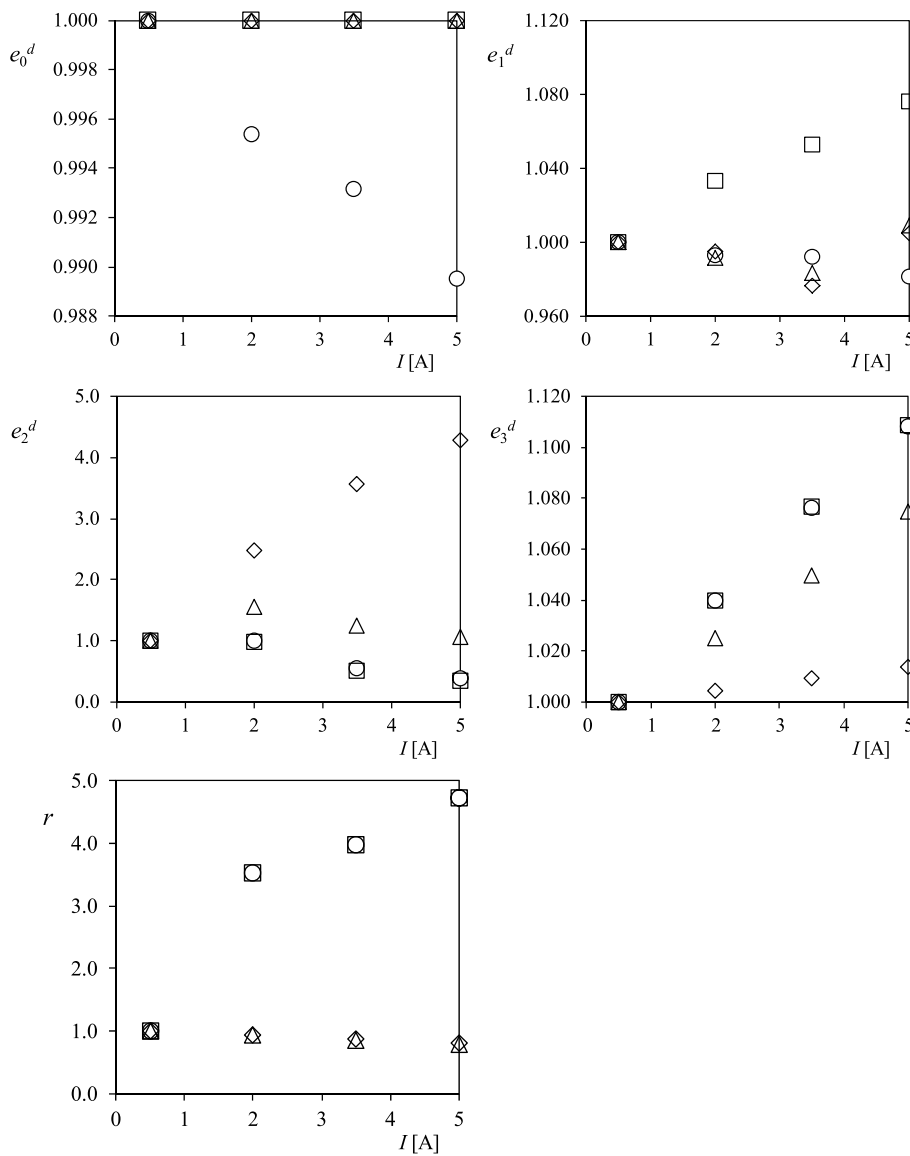


**Fig. 8.** Non-dimensional coefficients,  $e_0^d = E_0^d/E_0^d|_{I=0.5}$ ,  $e_1^d = E_1^d/E_1^d|_{I=0.5}$ ,  $e_2^d = E_2^d/E_2^d|_{I=0.5}$ ,  $e_3^d = E_3^d/E_3^d|_{I=0.5}$ , and  $r = R_d/R_d|_{I=0.5}$ , obtained from the fittings of equation (23) (open circles), equation (23) with fixed value of coefficient  $E_0^d$  (open squares), equation (24) with fixed values of coefficients  $E_0^d$ ,  $E_{3,1}^d$ ,  $E_{3,2}^d$ ,  $R_{d,0}$  and  $R_{d,1}$  (open triangles), and equation (25) with fixed values of all coefficients except  $E_1^d$  (open rhombi), to the Li-ion battery analyzed, plotted in relation to the discharging current,  $I$ .

the following equation, with a linear approach to coefficients  $E_3^d$  and  $R_d$  was fitted to all curves (see results in Table 3):

$$V(\phi, I) = E_0^d + E_1^d \phi + E_2^d \exp\left(\left(E_{3,0}^d + E_{3,1}^d I\right) \phi\right) - (R_{d,0} + R_{d,1} I) I. \quad (24)$$

This equation fits better to all curves than the previous one, showing a lower value of RMSE (see Fig. 7). Again, the pattern of coefficients  $E_1^d$  and  $E_2^d$  was analyzed by fitting the above equation to each curve but fixing coefficients  $E_0^d$ ,  $E_{3,0}^d$ ,  $E_{3,1}^d$ ,  $R_{d,0}$  and  $R_{d,1}$  at the values previously obtained (see Table 3). The results have been included in the graphs of Fig. 8 (open triangles). Coefficient  $E_2^d$  seems to follow a higher order polynomial pattern, whereas coefficient  $E_1^d$  changes its slope once more. As a result, a quadratic approach to  $E_2^d$  was suggested:

$$\begin{aligned} V(\phi, I) = & E_0^d + E_1^d \phi + \left(E_{2,0}^d + E_{2,1}^d I + E_{2,2}^d I^2\right) \exp\left(\left(E_{3,0}^d + E_{3,1}^d I\right) \phi\right) - (R_{d,0} \\ & + R_{d,1} I) I, \end{aligned} \quad (25)$$

and fitted to all curves (see Table 3), the RMSE being improved again (Fig. 7).

Following the procedure described above, equation (25) was fitted to each one of the discharging curves, fixing all coefficients at the values

previously obtained (see Table 2) with the exception of coefficient  $E_1^d$ . The results, included in the graphs of Fig. 8 (open rhombi) indicate a quadratic behavior of coefficient  $E_1^d$ , rather than a linear one. Consequently, the following equation was proposed as the logical evolution from equation (25):

$$\begin{aligned} V(\phi, I) = & E_0^d + \left(E_{1,0}^d + E_{1,1}^d I + E_{1,2}^d I^2\right) \phi + \left(E_{2,0}^d + E_{2,1}^d I + E_{2,2}^d I^2\right) \exp\left(\left(E_{3,0}^d \right. \right. \\ & \left. \left. + E_{3,1}^d I\right) \phi\right) - (R_{d,0} + R_{d,1} I) I, \end{aligned} \quad (26)$$

As in previous cases, this equation fits better than the previous ones to all curves (see Table 3), the RMSE being improved (Fig. 7).

Furthermore, a fifth term was included in the model to adjust the exponential behavior at the higher levels of discharged energy. This is quite important, as the voltage drops quickly at these higher levels of discharged energy, involving the risk of a too deep discharge that might damage the battery permanently (the output voltage of any Li-ion cell should not drop below 2.7 V [54]). Two expressions inside the exponential term of the model were studied, a potential one:

**Table 3**Coefficients of Equations (23)–(28), fitted to all discharging curves,  $I = 0.5, 2, 3.5$ , and  $5 \text{ A}$  (see Fig. 7).

Coefficient/RMSE	Eq. (23)	Eq. (24)	Eq. (25)	Eq. (26)	Eq. (27)	Eq. (28)	Eq. (28) <sup>c</sup>
$E_0^d [\text{V}]$	24.202	24.405	24.405	24.405	24.405	24.405	24.405
$E_1^d [\text{V}\cdot\text{W}^{-1}\text{ h}^{-1}]$	-1.2747·10 <sup>-2</sup>	-1.2462·10 <sup>-2</sup>	-1.2403·10 <sup>-2</sup>	-	-	-	-
$E_{1,0}^d [\text{V}\cdot\text{W}^{-1}\text{ h}^{-1}]$	-	-	-	-1.2654·10 <sup>-2</sup>	-1.2651·10 <sup>-2</sup>	-1.2654·10 <sup>-2</sup>	-1.2630·10 <sup>-2</sup>
$E_{1,1}^d [\text{V}\cdot\text{W}^{-1}\text{ h}^{-1}\text{ A}^{-1}]$	-	-	-	2.6180·10 <sup>-4</sup>	2.5732·10 <sup>-4</sup>	1.8426·10 <sup>-4</sup>	-7.5550·10 <sup>-5</sup>
$E_{1,2}^d [\text{V}\cdot\text{W}^{-1}\text{ h}^{-1}\text{ A}^{-2}]$	-	-	-	-5.8855·10 <sup>-5</sup>	-5.7924·10 <sup>-5</sup>	-4.5741·10 <sup>-5</sup>	3.8995·10 <sup>-5</sup>
$E_2^d [\text{V}]$	-7.6943·10 <sup>-14</sup>	-1.0029·10 <sup>-12</sup>	-	-	-	-	-
$E_{2,0}^d [\text{V}]$	-	-	-4.0145·10 <sup>-13</sup>	-5.8306·10 <sup>-14</sup>	-5.3141·10 <sup>-14</sup>	-6.4471·10 <sup>-15</sup>	-2.0344·10 <sup>-13</sup>
$E_{2,1}^d [\Omega]$	-	-	-1.1174·10 <sup>-12</sup>	-3.5520·10 <sup>-13</sup>	-3.6769·10 <sup>-13</sup>	-5.5915·10 <sup>-14</sup>	9.1348·10 <sup>-13</sup>
$E_{2,2}^d [\Omega\cdot\text{A}^{-1}]$	-	-	7.8076·10 <sup>-14</sup>	-5.9118·10 <sup>-14</sup>	-3.5307·10 <sup>-14</sup>	-2.4597·10 <sup>-14</sup>	7.1718·10 <sup>-14</sup>
$E_3^d [\text{W}^{-1}\text{ h}^{-1}]$	8.6289·10 <sup>-2</sup>	-	-	-	-	-	-
$E_{3,0}^d [\text{W}^{-1}\text{ h}^{-1}]$	-	7.8366·10 <sup>-2</sup>	7.8819·10 <sup>-2</sup>	8.2773·10 <sup>-2</sup>	8.2773·10 <sup>-2</sup>	8.2773·10 <sup>-2</sup>	7.9826·10 <sup>-2</sup>
$E_{3,1}^d [\text{W}^{-1}\text{ h}^{-1}\text{ A}^{-1}]$	-	1.3097·10 <sup>-3</sup>	2.3969·10 <sup>-4</sup>	-4.7173·10 <sup>-4</sup>	-3.6056·10 <sup>-4</sup>	-4.9042·10 <sup>-4</sup>	-1.1091·10 <sup>-4</sup>
$E_{4,1}^d [\text{W}^{-Ed4,2}\text{ h}^{-Ed4,2}]a$	-	-	-	-	1.0000·10 <sup>-5</sup>	-	-
$E_{4,2}^da$	-	-	-	-	1.0000·10 <sup>-5</sup>	-	-
$E_{4,1}^db$	-	-	-	-	-	1.3923·10 <sup>-2</sup>	1.3923·10 <sup>-2</sup>
$E_{4,2}^db$	-	-	-	-	-	1.3593·10 <sup>-2</sup>	9.9929·10 <sup>-3</sup>
$R_d [\Omega]$	5.7225·10 <sup>-2</sup>	-	-	-	-	-	-
$R_{d,0} [\Omega]$	-	1.7082·10 <sup>-1</sup>	1.343·10 <sup>-1</sup>				
$R_{d,1} [\Omega\cdot\text{A}^{-1}]$	-	-7.7198·10 <sup>-3</sup>	-6.8852·10 <sup>-3</sup>	-9.6168·10 <sup>-3</sup>	-9.6168·10 <sup>-3</sup>	-9.6168·10 <sup>-3</sup>	-9.29788·10 <sup>-3</sup>
RMSE [V]	2.9348·10 <sup>-1</sup>	1.2271·10 <sup>-1</sup>	1.0324·10 <sup>-1</sup>	1.0057·10 <sup>-1</sup>	1.0021·10 <sup>-1</sup>	9.2978·10 <sup>-2</sup>	9.4474·10 <sup>-2</sup>

<sup>a</sup> Equation (27).<sup>b</sup> Equation (28).<sup>c</sup> Coefficients of equation (28) after iterated recalculations of the discharged energy,  $\phi$ .**Table 4**

Coefficients of equation (29) model for the battery charging process, in relation to each one of the discharging curves (see also Fig. 9).

Coefficient/RMSE	$I = 0.5 \text{ A}$	$I = 1 \text{ A}$	$I = 2.5 \text{ A}$	$I = 3.5 \text{ A}$
$E_0^c [\text{V}]$	24.452	23.994	23.247	21.980
$E_1^c [\text{V}\cdot\text{W}^{-1}\text{ h}^{-1}]$	-1.2319·10 <sup>-2</sup>	-1.2103·10 <sup>-2</sup>	-1.1995·10 <sup>-2</sup>	-1.1835·10 <sup>-2</sup>
$E_2^c [\text{V}]$	-2.4245·10 <sup>-14</sup>	-5.8215·10 <sup>-15</sup>	-1.4387·10 <sup>-13</sup>	-1.1272·10 <sup>-15</sup>
$E_3^c [\text{W}^{-1}\text{ h}^{-1}]$	8.2694·10 <sup>-2</sup>	8.4728·10 <sup>-2</sup>	8.8489·10 <sup>-2</sup>	9.0428·10 <sup>-2</sup>
$R_c [\Omega]$	1.4558·10 <sup>-2</sup>	2.7752·10 <sup>-1</sup>	6.2727·10 <sup>-1</sup>	8.2841·10 <sup>-1</sup>
RMSE [V]	8.939·10 <sup>-2</sup>	5.130·10 <sup>-2</sup>	5.590·10 <sup>-2</sup>	5.050·10 <sup>-2</sup>

$$V(\phi, I) = E_0^d + (E_{1,0}^d + E_{1,1}^d I + E_{1,2}^d I^2) \phi + (E_{2,0}^d + E_{2,1}^d I + E_{2,2}^d I^2) \exp((E_{3,0}^d + E_{3,1}^d I) \phi + E_{4,1}^d \exp(E_{4,2}^d)) - (R_{d,0} + R_{d,1} I) I, \quad (27)$$

and an exponential one:

$$V(\phi, I) = E_0^c + (E_{1,0}^c + E_{1,1}^c I + E_{1,2}^c I^2) \phi + (E_{2,0}^c + E_{2,1}^c I + E_{2,2}^c I^2) \exp((E_{3,0}^c + E_{3,1}^c I) \phi + E_{4,1}^c \exp(E_{4,2}^c \phi)) - (R_{d,0} + R_{d,1} I) I. \quad (28)$$

The values of the constants corresponding to the fittings of the above equations to all discharging curves have been included in Table 3. Besides, the RMSE values of these two equations are shown in Fig. 7. It seems that equation (28) shows the better fitting to all discharging curves, though for the larger discharging rates its RMSE values are larger than the ones obtained by fitting equation (23) to each curve individually. However, the error value of equation (28) when fitted to all curves is equal to the averaged value of the error obtained in the fittings of equation (23) to each curve individually. In Fig. 7, the fittings of equation (28) model are shown.

Finally, with the calculated values of the resistor from equation (28) (see Table 3), the discharged energy,  $\phi$ , has been recalculated for every point of the discharging curves, generating new curves  $V-\phi$  and new values of the model parameters. Four iterations were carried out to analyze the convergence to a stable solution. The results showed a very fast convergence with very low percentage differences between the coefficient values from two consecutive iterations.

### 3.3. Charging process

With regard to the charging process, the methodology followed is similar to the one from the previous subsection. In Table 4, the results related to the fittings of the model for the battery internal voltage charging process:

$$V(\phi, I) = E_0^c + E_1^c \phi + E_2^c \exp(E_3^c \phi) + R_c I, \quad (29)$$

to the experimental curves once translated to output voltage related to discharged energy rate,  $\phi$  (see Fig. 9). It can be observed that the coefficients of the above expression are quite similar to the ones obtained from the discharging process (Table 2), with the exception of coefficient  $E_2^c$ , which order of magnitude seems to be much lower. The initial equation consists of linear terms (offset and slope) plus an exponential one that reflects the behavior when the battery is almost fully discharged.

As carried out within the analysis of the discharging process, the extracted coefficients from Table 4, were made non-dimensional with their own values at  $I = 0.5$ ,  $e_0^c = E_0^c/E_3^c|_{I=0.5}$ ,  $e_1^c = E_1^c/E_3^c|_{I=0.5}$ ,  $e_2^c = E_2^c/E_3^c|_{I=0.5}$ ,  $e_3^c = E_3^c/E_3^c|_{I=0.5}$ , and  $r = R_c/R_c|_{I=0.5}$ , and plotted as a function of the discharging current,  $I$ , in Fig. 10. As proceeded also in the previous subsection, the calculations of the discharged energy rate,  $\phi$ , with equation (19), were carried out taking into account a constant value of the internal resistor  $R_c = 0.1591 \Omega$ , extracted from an initial estimation. In case of the charging, all coefficients (including the series resistor) seem to have a linear relationship with the current, with the exception of coefficient  $E_2^c$ , which shows a higher order dependence on the current (quadratic, potential ...). In order to follow an organized procedure, equation was fitted (29) to all data (that is, to all charging curves), the results being included in Table 5. After that, and taking into account the

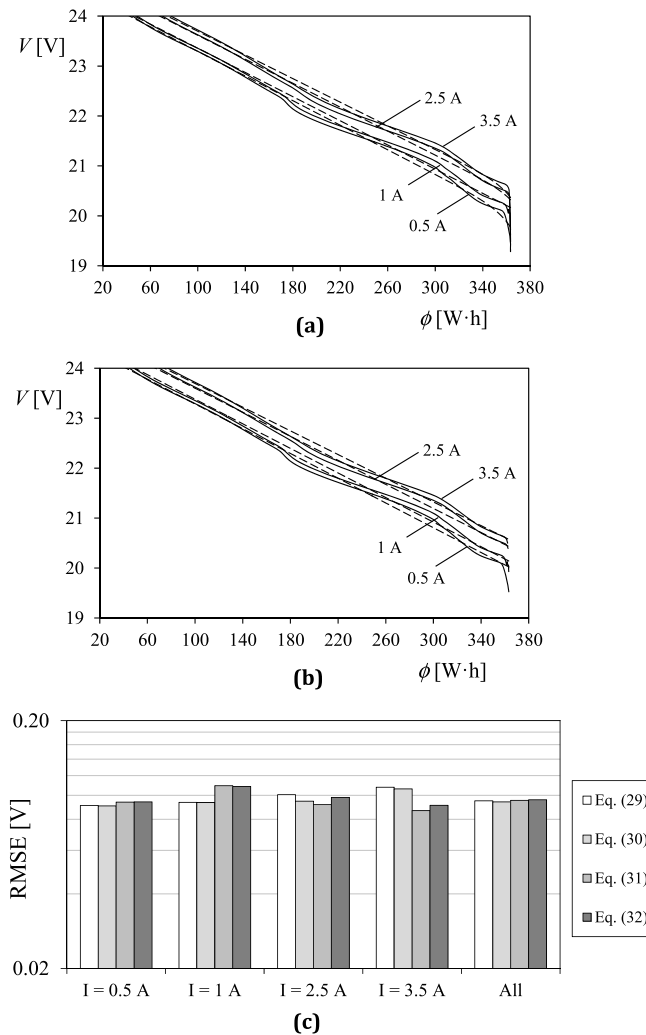


**Fig. 9.** Charging curves of the tested battery: (a) fittings of equation (29) to each one of the curves (see also the coefficients corresponding to each fitting in Table 4), and (b) fittings of equation (32) to all curves (see Table 5). (c) RMSE of the analyzed battery charging models (results from equations (29)–(32) fitted to all currents data –see Table 5–).

linear behavior of the series resistor with the current, the following equation was fitted to the data (that is to all curves):

$$V(\phi, I) = E_0^c + E_1^c \phi + E_2^c \exp(E_3^c \phi) + (R_{c,0} + R_{c,1} I) I. \quad (30)$$

The resulting coefficients are included in Table 5 (see also Fig. 9). The RMSE is slightly improved in relation to equation (29). After that, equation (30) was fitted sequentially to each one of the charging curves setting the values  $E_0^c$ ,  $R_{c,0}$  and  $R_{c,1}$  at the figures previously obtained. The non-dimensional coefficients  $e_1^c$ ,  $e_2^c$  and  $e_3^c$  resulting from these fittings are included in Fig. 10. Bearing in mind the low values obtained of coefficient  $E_2^c$ , and the quadratic pattern observed in relation to  $e_1^c$ , the following equation was then fitted to all data:

$$V(\phi, I) = E_0^c + (E_{1,0}^c + E_{1,1}^c I + E_{1,2}^c I^2) \phi + (R_{c,0} + R_{c,1} I) I, \quad (31)$$

the results being included in Table 5. The non-dimensional coefficients have been included in Fig. 10. The RMSE resulting from the above equation (see Table 5) does not improve the one obtained from equation (30). A last fitting was carried out, reducing the second term to a linear equation:

$$V(\phi, I) = E_0^c + (E_{1,0}^c + E_{1,1}^c I) \phi + (R_{c,0} + R_{c,1} I) I. \quad (32)$$

The results do not improve the RMSE. However, this expression was selected to continue the present work, as it is simpler than the other ones without representing a relevant decrease of the accuracy.

### 3.4. Dynamic discharging/charging process

Finally, the dynamic behavior of the model was simulated (Fig. 11). A discharging process at  $I = 2$  A was programmed, with a 20-step dynamic discharging/charging process each hour. This 20-step process is plotted in Fig. 11, together with the measured battery output voltage. Based on this measured the complete model from static and dynamic processes from Fig. 11 was fitted to the data. Based on this work the following parameters were extracted:  $R_1 = 9.5428 \cdot 10^{-2} \Omega$ ,  $R_2 = 2.3717 \cdot 10^{-2} \Omega$ ,  $C_1 = 70468.7 \text{ F}$ ,  $C_2 = 252.581 \text{ F}$ ,  $R_{int} = 5.2491 \cdot 10^{-2} \Omega$ . Besides, the remaining resistor term was simplified to  $R_c - R_d = 5.2491 \cdot 10^{-2} \Omega$ . In the aforementioned Fig. 11, the simulated voltage level is included.

## 4. Modeling the UPMSat-2 power system

A simplified model of the UPMSat-2 power distribution system is sketched in Fig. 12. This distribution system is based on a DET configuration, the solar panels being directly connected to the battery. The distribution is channeled to the payloads, P/L, through the BUS and the  $\pm 15$  V DC/DC converter, the +5 and + 3.3 DC/DC converters being connected to the later. The possibility of using a Maximum Power Point Tracking (MPPT) system is indicated in the figure with dashed line.

As indicated in Section 2.1 of the present work, the MPPT is basically a DC/DC converter that corrects the voltage level at the primary side to set it at the Maximum Power Point (MPP) related to the solar panels, that is, at  $V_{mp}$ . It should be also mentioned that each solar panel requires its own DC/DC converter (this fact increasing the complexity of the system and, as a consequence, the possibility of failure). The UPMSat-2 operates in a 10:30 Sun-synchronous orbit at 525 km altitude, the  $z$  axis being perpendicular to the orbit's plane thanks to the magnetic Attitude Determination and Control Subsystem (ADCS). The satellite rotates around its  $z$  axis [16], the rotation rate being around  $w = 0.02 \text{ rad/s}$  (see Fig. 13).

The power subsystem is studied in the present work under the following constraints:

- Only 1 day (15 orbits of 90 min) is analyzed, the power consumptions by the different payloads, P/L, being defined in Table 6 (see also Fig. 14). These consumptions are extracted from the planned mission of the UPMSat-2, the experiments being related to Shape Memory Alloys (Exp. 1), Microthermal Switch (Exp. 2), and a Reaction Wheel (Exp. 3).
- Bearing in mind the attitude of the spacecraft, only lateral panels are sequentially irradiated by the Sun.
- The satellite's rotation rate considered is  $w = 0.02 \text{ rad/s}$ .
- The solar panel behavior is calculated with the Pindado & Cubas model instead of the 1-D/2-R equivalent circuit model due to both its simplicity and accuracy (see Section 2).
- The solar panels are composed by 4 parallel-connected strings composed of 10-series connected 3G28C Azur Space solar cells (see Table 7).
- The battery model considered is the one from Section 3, its initial state was the corresponding to  $V = 22.9 \text{ V}$  voltage level (corresponding to  $\phi = 130.18 \text{ W h}$  energy discharged level, see equations (18) and (19)). Normally, the state of spacecraft batteries at the beginning of a mission is not fully charged, as integration with the launcher and possible delays due to weather conditions should be taken into account (this was the case of the UPMSat-2).

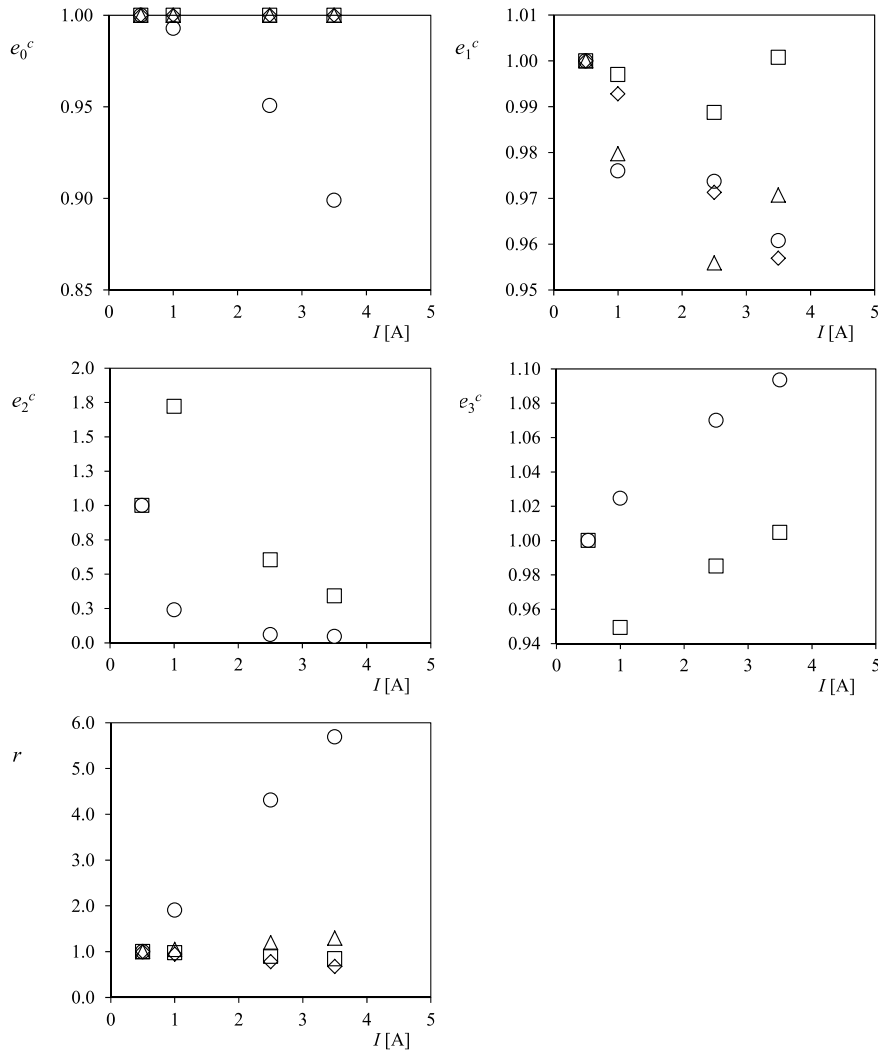


**Fig. 10.** Non-dimensional coefficients,  $e_0^c = E_0^c/E_0^c|_{I=0.5}$ ,  $e_1^c = E_1^c/E_1^c|_{I=0.5}$ ,  $e_2^c = E_2^c/E_2^c|_{I=0.5}$ ,  $e_3^c = E_3^c/E_3^c|_{I=0.5}$ , and  $r = R_c/R_c|_{I=0.5}$ , obtained from the fittings of equation (29) (open circles), equation (30) with fixed values of  $E_0^c$ ,  $E_2^c$ ,  $E_3^c$ ,  $R_{c,0}$  and  $R_{c,1}$  (open squares), equation (31) (open triangles) and equation (32) (open rhombi) to the Li-ion battery analyzed, plotted in relation to the discharging current,  $I$ .

**Table 5**

Coefficients of battery charging equations (29)–(32), fitted to all experimental data (see also Fig. 9).

Coefficient/RMSE	Eq. (29)	Eq. (30)	Eq. (31)	Eq. (32)	Eq. (32) <sup>a</sup>
$E_0^c$ [V]	24.420	24.402	24.489	24.431	24.437
$E_1^c$ [ $\text{V}\cdot\text{W}^{-1}\text{h}^{-1}$ ]	$-1.2179\cdot10^{-2}$	$-1.2179\cdot10^{-2}$	–	–	–
$E_{1,0}^c$ [ $\text{V}\cdot\text{W}^{-1}\text{h}^{-1}$ ]	–	–	$-1.2776\cdot10^{-2}$	$-1.2485\cdot10^{-2}$	$-1.2528\cdot10^{-2}$
$E_{1,1}^c$ [ $\text{V}\cdot\text{W}^{-1}\text{h}^{-1}\text{A}^{-1}$ ]	–	–	$7.3391\cdot10^{-4}$	$1.7806\cdot10^{-4}$	$2.370\cdot10^{-4}$
$E_{1,2}^c$ [ $\text{V}\cdot\text{W}^{-1}\text{h}^{-1}\text{A}^{-2}$ ]	–	–	$-1.5311\cdot10^{-4}$	–	–
$E_2^c$ [V]	$-9.8614\cdot10^{-14}$	$-3.1743\cdot10^{-14}$	–	–	–
$E_3^c$ [ $\text{W}^{-1}\text{h}^{-1}$ ]	$7.7992\cdot10^{-2}$	$8.1177\cdot10^{-2}$	–	–	–
$R_c$ [ $\Omega$ ]	$1.6143\cdot10^{-1}$	–	–	–	–
$R_{c,0}$ [ $\Omega$ ]	–	$1.9740\cdot10^{-1}$	$9.2333\cdot10^{-2}$	$2.0241\cdot10^{-1}$	$2.0241\cdot10^{-1}$
$R_{c,1}$ [ $[\Omega\text{A}^{-1}]$ ]	–	$-1.0219\cdot10^{-2}$	$9.5179\cdot10^{-3}$	$-2.0916\cdot10^{-2}$	$-2.5249\cdot10^{-2}$
RMSE [V]	$9.489\cdot10^{-2}$	$9.410\cdot10^{-2}$	$9.540\cdot10^{-2}$	$9.597\cdot10^{-2}$	$9.489\cdot10^{-2}$

<sup>a</sup> Coefficients of equation (32) after iterated recalculations of the discharged energy,  $\phi$ .

- Finally, Beginning Of Life (BOL) is considered (that is, no degradation of the solar panels –due to irradiance accumulation– or the battery –due to charge/discharge cycling– is taken into account).

The simulations were programmed in Matlab®. The first simulation carried out was the corresponding to DET power distribution configuration, that is, the solar panels work permanently at the voltage

established by the battery. As the Pindado & Cubas model is used, the characteristic points of the solar panels are required. These characteristic points are derived from the information given by the manufacturer in relation to one single solar cell (multiplying currents at short circuit and maximum power points by 4, and voltages levels at maximum power and open circuit points by 10) at Standard Test Conditions (STC), and equations (13)–(16), to take into account the variations of

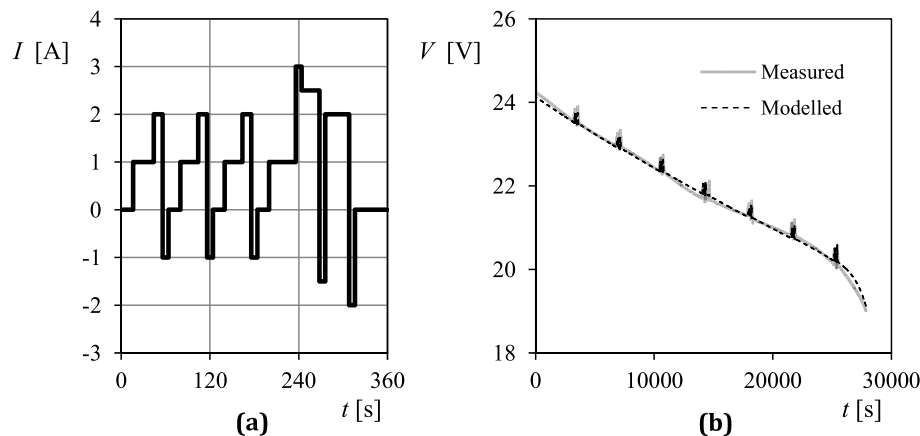


**Fig. 11.** (a) 20-step dynamic discharging/charging process programmed to test the studied model when fitting the dynamic behavior of a Li-Ion battery. (b) Discharging process at 2 A combined with intervals of the 20-step dynamic discharging/charging process each hour.

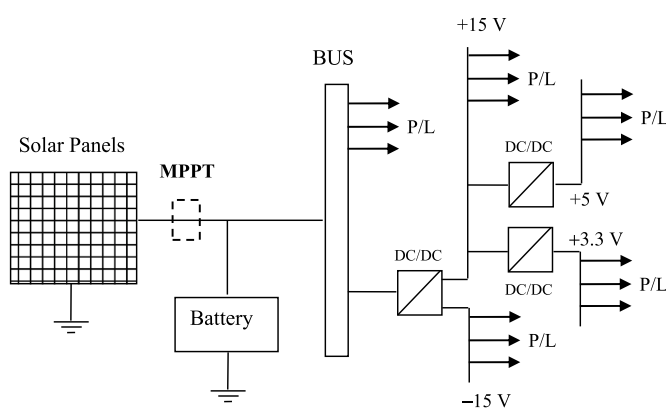


**Fig. 12.** Simplified model of the UPMSat-2 power distribution subsystem. The location of the MPPT analyzed in the present work is indicated in the figure with dashed line (there is one MPPT for each solar panel).

irradiance,  $G$ , and temperature,  $T$  (see all data required in Table 7). Based on the thermal analyses carried out with ESATAN© [23], the following temperature profiles for daylight period and eclipse have been respectively defined for this simulation (see Fig. 15):

$$T = -10.8 + 41.6(1 - \exp(-1.1043 \cdot 10^{-3}(t - t_d))), \quad (33)$$

$$T = 29.8 - 44.8 \left( 1 - \exp \left( -\sqrt{1.2478 \cdot 10^{-6}(t - t_e)^2 + 2.7616 \cdot 10^{-4}(t - t_e)} \right) \right), \quad (34)$$

where  $t_d$  and  $t_e$  are the beginning times for daylight period and eclipse within the orbit.

The evolution of the battery voltage and its current rates resulting from this simulation is plotted in Fig. 16. Additionally, the discharged energy (that reflects the state of discharge of the battery), and the power extracted from the panels are plotted in Fig. 17. The graphs of these figures indicate that after an initial discharge of the battery due to the

**Table 6**

UPMSat-2 subsystems and data transmission (D.T.), and three experiments: Experiment 1, Experiment 2, and Experiment 3 power demand within the analyzed 15 orbits (1 day), see also Fig. 14.

Consumption	Operation [s]	BUS [W]	+15 V [W]	-15 V [W]	+5 V [W]	+3.3 V [W]
Mission	constant	5.358	0.4370	0.1870	1.258	3.603
D.T.	600 <sup>a</sup>	5.7	–	–	–	–
Exp. 1	600	110	–	–	–	–
Exp. 2(a)	10800	7.3	–	–	–	–
Exp. 2(b)	26190	18.3	–	–	–	–
Exp. 3	1200	18	–	–	0.5	–

<sup>a</sup> Two times per orbit.

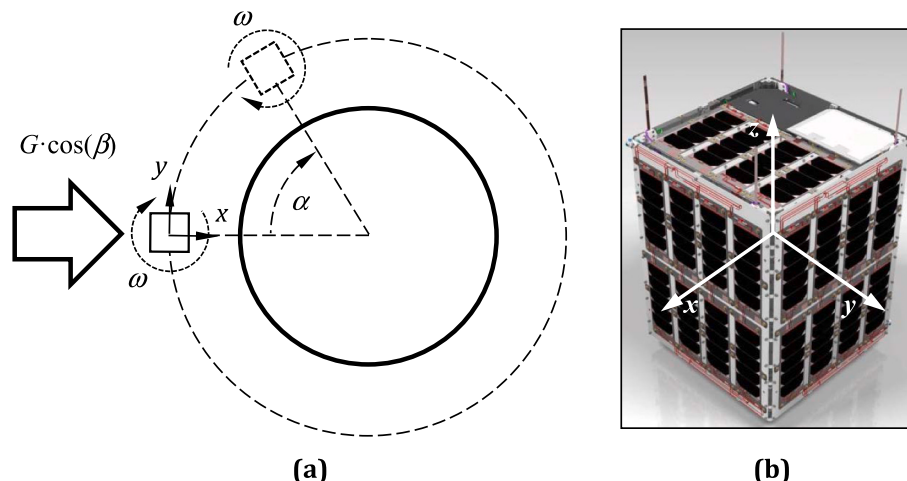


**Fig. 13.** (a) Sketch of the UPMSat-2 attitude within the 10:30 Sun-synchronous orbit (with  $\beta = 22.5^\circ$  inclination with regard to Sun irradiance). (b) UPMSat-2 reference axes.

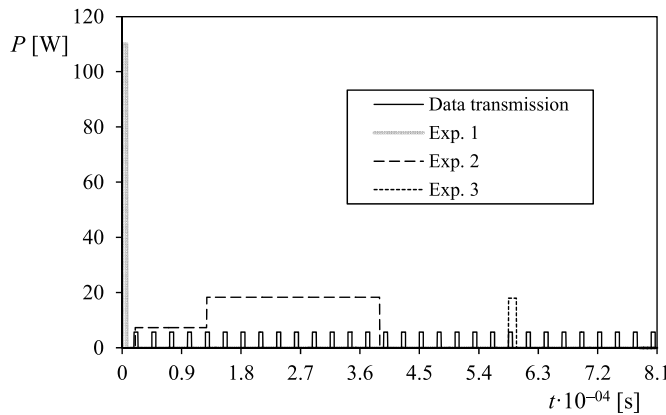


Fig. 14. UPMSat-2 P/L power consumption (see also Fig. 12).

**Table 7**  
Characteristics of 3G28C Azur Space solar cell and the UPMSat-2 lateral solar panels.

Parameter	3G28C solar cell	UPMSat-2 solar panel
$V_{oc}$ [V]	2.667	26.67
$I_{sc}$ [A]	0.506	2.024
$V_{mp}$ [V]	2.371	23.71
$I_{mp}$ [A]	0.487	1.948
$\alpha_{voc}$ [mV/ $^{\circ}$ C]	-6.0	-60
$\alpha_{isc}$ [mA/ $^{\circ}$ C]	0.32	1.28
$\alpha_{vmp}$ [mV/ $^{\circ}$ C]	-6.1	-61
$\alpha_{imp}$ [mA/ $^{\circ}$ C]	0.28	1.12

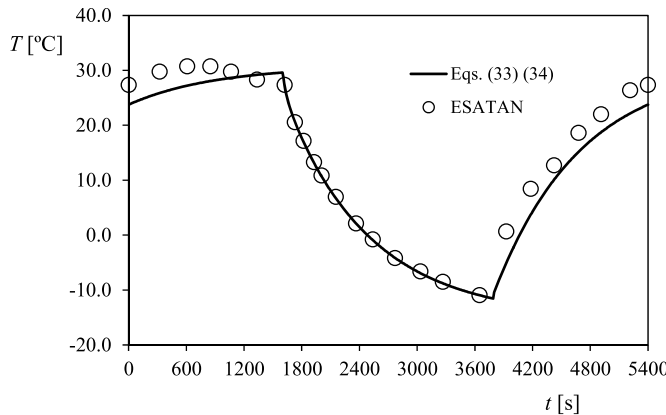


Fig. 15. UPMSat-2 lateral panels averaged (on one rotation around z-axis) temperature,  $T$ , along one orbit. In the graph, the temperature modeled with equations (33) and (34) is compared to the results from ESATAN simulations.

large power demand from the Experiment 1, it recovers progressively close to full-charge state at the end of the 15-orbit period. Besides, the current rates of the battery are below 2 A, with the exception of the period in which Experiment 1 is demanding power (which force the battery to a 3.8 A current supply). Finally, the power supply from the solar panels is between 41W and 59.5 W approximately during daylight period, the total amount of energy transferred being  $E_{sp} = 2.56 \cdot 10^{+06}$  J during the studied 15-orbit period. It should be underlined the large amount of energy supplied by the solar panels with the studied DET configuration, as it represent a 96.9% of the maximum (represented by fixing the operation point of the solar panels at MPP). This is possible as the solar panels working point, fixed by the battery voltage is always close to the MPP of the corresponding I-V curve.

In order to study the effect of a MPPT configuration, the MPPT sys-

tem was modeled as a DC-DC converter characterized by equation (17), the current function,  $f(I)$ , being defined by one constant, the characteristic current  $I_{ch}$ :

$$f(I) = -\frac{I}{I_{ch}}. \quad (35)$$

Therefore, the current transferred from one of the UPMSat-2 solar panels and after the MPPT system,  $I_{sp}$ , can be expressed as:

$$I_{sp} = \frac{V_{mp} I_{mp}}{V_{batt}} \eta, \quad (36)$$

where  $V_{batt}$  is the voltage level of the battery and  $\eta$  is the efficiency of the MPPT system. Bearing in mind equations (17) and (35), the above equation can be derived into the following explicit expression:

$$I_{sp} = \frac{V_{mp} I_{mp}}{V_{batt}} \eta_{max} \left( 1 - \exp \left( -\frac{I_{sp}}{I_{ch}} \right) \right), \quad (37)$$

that can be solved by using the Lambert W-function, and more precisely its positive branch  $W_0$ :

$$I_{sp} = I_{ch} (\lambda + W_0(-\lambda \exp(-\lambda))), \quad (38)$$

where:

$$\lambda = \frac{V_{mp} I_{mp}}{V_{batt} I_{ch}} \eta_{max}. \quad (39)$$

Four different maximum efficiencies  $\eta_{max} = 0.6, 0.7, 0.8$  and  $0.9$ , and eight different characteristic currents  $I_{ch} = 0.1, 0.2, 0.3, 0.4, 0.5, 0.6, 0.7$  and  $0.8$  A were analyzed. In Fig. 18, the performance of two of these cases (MPP-1, corresponding to  $\eta_{max} = 0.9$  and  $I_{ch} = 0.1$ , and MPP-2, corresponding to  $\eta_{max} = 0.7$  and  $I_{ch} = 0.5$ ) are shown and compared to the efficiencies of the DC-DC converters existing in the UPMSat-2 power distribution subsystem.

The results of the power subsystem simulations with the aforementioned MPPT cases are shown in Fig. 19. In the graph of this figure, the transferred energy from the solar panels in these simulations,  $E_{sp,MPPT}$ , made non-dimensional with the transferred energy in the DET simulation ( $E_{sp,DET} = 2.56 \cdot 10^{+06}$  J, as stated above),  $E_{sp,MPPT}/E_{sp,DET}$ , is plotted in relation to the characteristic current,  $I_{ch}$ , of the MPPT system. It can be observed that in all studied cases with MPPT system configuration, the amount of energy transferred from the solar panels is lower than the one resulting from the DET configuration. Additionally, in Fig. 20 the evolution of the battery voltage,  $V$ , and its discharged energy level,  $\varphi$ , in the aforementioned cases MPPT-1 and MPPT-2 have been plotted. In these graphs the evolutions of both variables can be compared to the ones from the DET case. As can be observed, in both cases, the battery is more discharged in relation to DET case as a result of a less efficient energy transfer from the solar panels.

## 5. Conclusions

In the present work the simplified simulation of a spacecraft power subsystem is carried out by integrating the simulations of:

- Solar panels.
- Battery.
- DC/DC converters.

The simulations are thoroughly described, their results indicating a very good agreement with experimental data from measurement campaigns designed at IDR/UPM Institute, and carried out within the research framework related to the UPMSat-2 spacecraft development.

A case study consisting in the power subsystem of the UPMSat-2 (successfully launched with the VV16 VEGA mission on September the 2nd 2020) was analyzed. The purpose of this case study was to compare the Direct Energy Transfer (DET) and Maximum Power Point Tracking

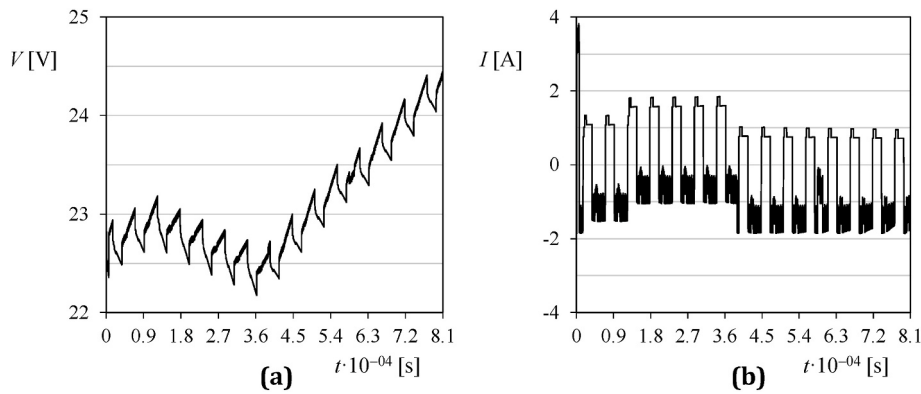


**Fig. 16.** UPMSat-2 power subsystem simulation (DET configuration) along 15 orbits (1 day). (a) Battery voltage. (b) Battery current rates (negative values correspond to battery charging rates).

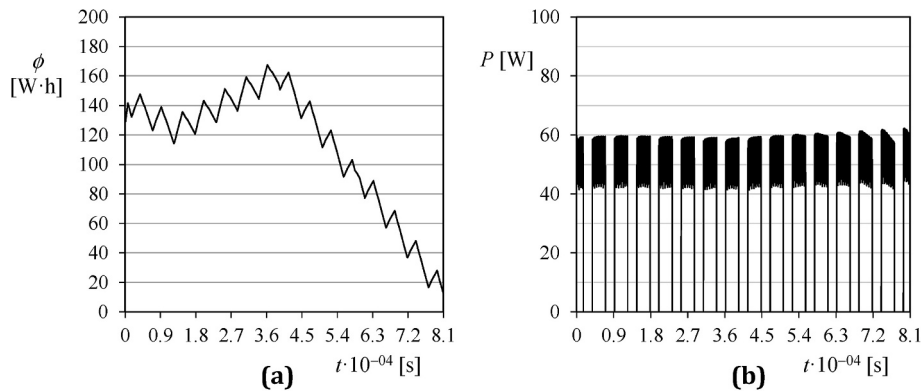


**Fig. 17.** UPMSat-2 power subsystem simulation (DET configuration) along 15 orbits (1 day). (a) Battery discharged energy. (b) Power supplied by the solar panels.

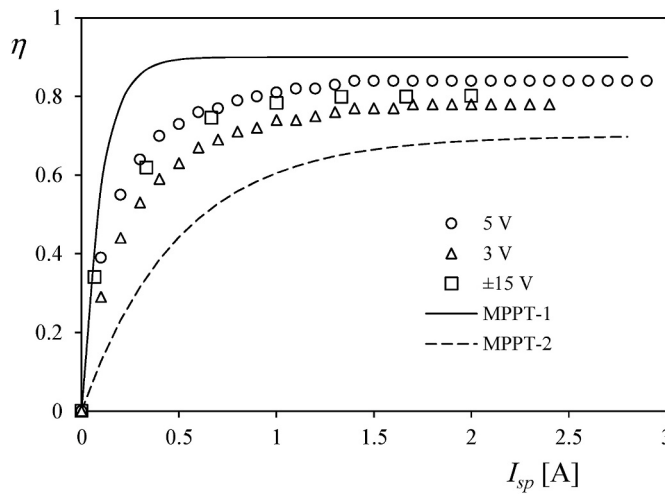


**Fig. 18.** MPPT-1 ( $\eta_{\max} = 0.9$  and  $I_{ch} = 0.1$ ) and MPPT-2 ( $\eta_{\max} = 0.7$  and  $I_{ch} = 0.5$ ) efficiencies in relation to the secondary current,  $I_{sp}$ , see equations (35)–(39). The efficiencies from the UPMSat-2 DC/DC converters have been included in the graph additionally (see Fig. 4).

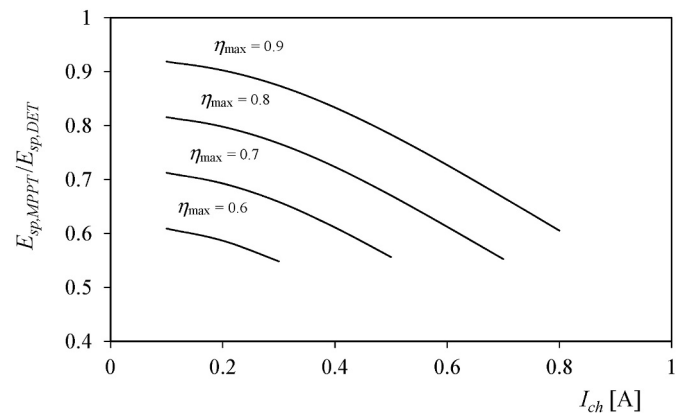


**Fig. 19.** Transferred energy from the solar panels in simulations of the UPMSat-2 power distribution system with MPPT related to the amount obtained in the simulation with DET configuration,  $E_{sp,MPPT}/E_{sp,DET}$ , is plotted with regard to the characteristic current,  $I_{ch}$ , of the MPPT system.

performance in LEO mission satellites of DET configuration when compare to MPPT ones.

#### Declaration of competing interest

The authors declare that they have no known competing financial interests or personal relationships that could have appeared to influence the work reported in this paper.

(MPPT) configurations in the UPMSat-2 power subsystem configuration. The results indicate a higher level of transferred energy from the solar panels in the case of DET configuration. This fact together with the more simplicity of this configuration (less amount of parts subjected to possible failure during the mission), seems to indicate a better

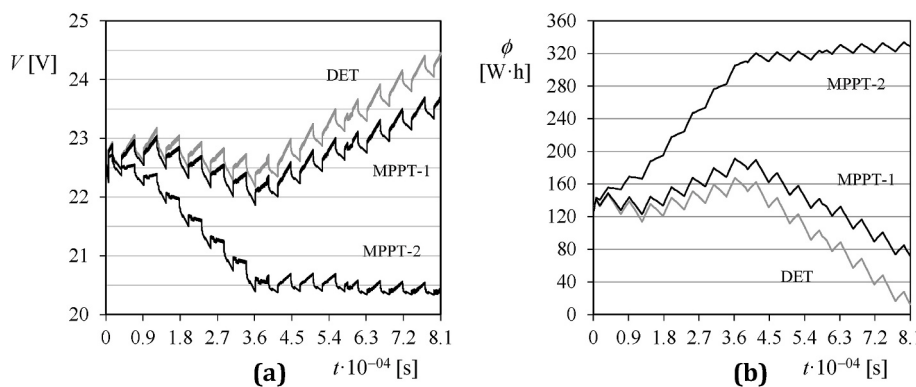


**Fig. 20.** (a) Battery voltage,  $V$ , and (b) discharged energy level,  $\phi$ , during the simulations of the UPMSat-2 power subsystem equipped with MPPT-1 ( $\eta_{\max} = 0.9$  and  $I_{ch} = 0.1$ ) and MPPT-2 ( $\eta_{\max} = 0.7$  and  $I_{ch} = 0.5$ ) systems (see Fig. 18).

## Acknowledgements

The authors are indebted to Prof. Ángel Sanz-Andrés for his constant support regarding the research program on spacecraft power subsystems at *Instituto Universitario de Microgravedad “Ignacio Da Riva”* (IDR/UPM), from Universidad Politécnica de Madrid (UPM). The authors are also grateful to the Reviewers whose comments helped to improve the present work.

## References

- [1] G. Fernández-Rico, I. Pérez-Grande, A. Sanz-Andrés, I. Torralbo, J. Woch, Quasi-autonomous thermal model reduction for steady-state problems in space systems, *Appl. Therm. Eng.* 105 (2016) 456–466, <https://doi.org/10.1016/j.applthermeng.2016.03.017>.
- [2] A. García-Pérez, F. Sorribes-Palmer, G. Alonso, A. Ravanbakhsh, Overview and application of FEM methods for shock analysis in space instruments, *Aero. Sci. Technol.* 80 (2018) 572–586, <https://doi.org/10.1016/j.ast.2018.07.035>.
- [3] A. Gómez-San-Juan, I. Pérez-Grande, A. Sanz-Andrés, Uncertainty calculation for spacecraft thermal models using a generalized SEA method, *Acta Astronaut.* 151 (2018) 691–702, <https://doi.org/10.1016/j.actaastro.2018.05.045>.
- [4] I. Torralbo, I. Pérez-Grande, A. Sanz-Andrés, J. Piqueras, Correlation of spacecraft thermal mathematical models to reference data, *Acta Astronaut.* 144 (2018) 305–319, <https://doi.org/10.1016/j.actaastro.2017.12.033>.
- [5] A. García-Pérez, A. Sanz-Andrés, G. Alonso, M. Chimeno Mangúan, Dynamic coupling on the design of space structures, *Aero. Sci. Technol.* 84 (2019) 1035–1048, <https://doi.org/10.1016/j.ast.2018.11.045>.
- [6] A. García-Pérez, F. Sorribes-Palmer, G. Alonso, A. Ravanbakhsh, FEM simulation of space instruments subjected to shock tests by mechanical impact, *Int. J. Impact Eng.* 126 (2019) 11–26, <https://doi.org/10.1016/j.ijimpeng.2018.12.008>.
- [7] J. Cubas, S. Pindado, M. Victoria, On the analytical approach for modeling photovoltaic systems behavior, *J. Power Sources* 247 (2014) 467–474, <https://doi.org/10.1016/j.jpowsour.2013.09.008>.
- [8] J. Cubas, S. Pindado, C. de Manuel, Explicit expressions for solar panel equivalent circuit parameters based on analytical formulation and the Lambert W-function, *Energies* 7 (2014) 4098–4115, <https://doi.org/10.3390/en7074098>.
- [9] J. Cubas, S. Pindado, C. de Manuel, New method for analytical photovoltaic parameters identification: meeting manufacturer's datasheet for different ambient conditions, in: A.Y. Oral, Z.B. Bahsi, M. Ozer (Eds.), *Int. Congr. Energy Effic. Energy Relat. Mater. (ENEFM2013)*, vol. 155, Springer International Publishing, Antalya, Turkey, 2014, pp. 161–169, <https://doi.org/10.1007/978-3-319-05521-3>. Springer Proc. Phys.
- [10] J. Cubas, S. Pindado, A. Sanz-Andrés, Accurate simulation of MPPT methods performance when applied to commercial photovoltaic panels, *Sci. World J.* (2015) 1–16, <https://doi.org/10.1155/2015/914212>, 2015.
- [11] J. Cubas, S. Pindado, F. Sorribes-Palmer, Analytical calculation of photovoltaic systems maximum power point (MPP) based on the operation point, *Appl. Sci.* 7 (2017) 1–15, <https://doi.org/10.3390/app7090870>.
- [12] E. Roibás-Millán, A. Alonso-Moragón, A. Jiménez-Mateos, S. Pindado, Testing solar panels for small-size satellites: the UPMSAT-2 mission, *Meas. Sci. Technol.* 28 (2017) 1–12, <https://doi.org/10.1088/1361-6501/aa85fc>.
- [13] S. Pindado, J. Cubas, Simple mathematical approach to solar cell/panel behavior based on datasheet information, *Renew. Energy* 103 (2017) 729–738, <https://doi.org/10.1016/j.renene.2016.11.007>.
- [14] S. Pindado, J. Cubas, E. Roibás-Millán, F. Bugallo-Siegel, F. Sorribes-Palmer, Assessment of explicit models for different photovoltaic technologies, *Energies* 11 (2018) 1–22, <https://doi.org/10.3390/en11061353>.
- [15] S. Pindado Carrion, E. Roibás-Millán, J. Cubas Cano, A. García, A.P. Sanz Andres, S. Franchini, M.I. Pérez Grande, G. Alonso, J. Pérez-Alvarez, F. Sorribes-Palmer, A. Fernandez-López, M. Ogueta-Gutierrez, I. Torralbo, J. Zamorano, J.A. de la Puente Alfaro, A. Alonso, J. Garrido, The UPMSat-2 Satellite: an academic project within aerospace engineering education, in: Athens ATINER'S Conf. Pap. Ser. No ENGEDU2017-2333, Athens Institute for Education and Research. ATINER, Athens, Greece, 2017, pp. 1–28.
- [16] J. Cubas, A. Farrahi, S. Pindado, Magnetic attitude control for satellites in polar or sun-synchronous orbits, *J. Guid. Contr. Dynam.* 38 (2015) 1947–1958, <https://doi.org/10.2514/1.G000751>.
- [17] A. Porras-Hermoso, S. Pindado, J. Cubas, Lithium-ion battery performance modeling based on the energy discharge level, *Meas. Sci. Technol.* 29 (2018) 1–6, <https://doi.org/10.1088/1361-6501/aae231>.
- [18] M. Bandecchi, B. Melton, F. Ongaro, Concurrent Engineering Applied to Space Mission Assessment and Design, *Esa Bull. Sp. Agency.*, 1999, pp. 34–40.
- [19] S.D. Wall, Use of concurrent engineering in space mission design, in: Proc. 2nd European Sist. Eng. Conf., 2000, pp. 1–6. <https://trs.jpl.nasa.gov/bitstream/handle/2014/15133/00-1144.pdf?sequence=1&isAllowed=true>.
- [20] A. Brakuhane, D. Quantius, Interactions in space systems design within a Concurrent Engineering facility, in: Proc. 2011 Int. Conf. Collab. Technol. Syst. CTS 2011, IEEE, 2011, pp. 381–388, <https://doi.org/10.1109/CTS.2011.5928714>.
- [21] A.B. Ivanov, L. Masson, F. Belloni, Operation of a concurrent design facility for university projects, in: 2016 IEEE Aerosp. Conf. Proc., IEEE, 2016, pp. 1–9, <https://doi.org/10.1109/AERO.2016.7500631>.
- [22] G. Loureiro, W.F. Panades, A. Silva, Lessons learned in 20 years of application of Systems Concurrent Engineering to space products, *Acta Astronaut.* 151 (2018) 44–52, <https://doi.org/10.1016/j.actaastro.2018.05.042>.
- [23] J. Cubas, A.M. Gomez-Sanjuan, S. Pindado, On the thermo-electric modelling of smallsats, in: 50th Int. Conf. Environ. Syst. – ICES 2020 (12–16 July 2020, 2020, pp. 1–12, Lisbon, Port., Lisbon, Portugal, <https://hdl.handle.net/2346/86449>.
- [24] D.T. Cotfas, P.A. Cotfas, S. Kaplanis, Methods to determine the dc parameters of solar cells: a critical review, *Renew. Sustain. Energy Rev.* 28 (2013) 588–596, <https://doi.org/10.1016/j.rser.2013.08.017>.
- [25] A. Ortiz-Conde, F.J. García-Sánchez, J. Muci, A. Sucre-González, A review of diode and solar cell equivalent circuit model lumped parameter extraction, *Facta Univ. – Ser. Electron. Energetics* 27 (2014) 57–102, <https://doi.org/10.2298/FUEI4010570>.
- [26] D. Jena, V.V. Ramana, Modeling of photovoltaic system for uniform and non-uniform irradiance: a critical review, *Renew. Sustain. Energy Rev.* 52 (2015) 400–417, <https://doi.org/10.1016/j.rser.2015.07.079>.
- [27] V.J. Chin, Z. Salam, K. Ishaque, Cell modelling and model parameters estimation techniques for photovoltaic simulator application: a review, *Appl. Energy* 154 (2015) 500–519, <https://doi.org/10.1016/j.apenergy.2015.05.035>.
- [28] A.M. Humada, M. Hojabri, S. Mekhilef, H.M. Hamada, Solar cell parameters extraction based on single and double-diode models: a review, *Renew. Sustain. Energy Rev.* 56 (2016) 494–509, <https://doi.org/10.1016/j.rser.2015.11.051>.
- [29] S. Yadir, R. Bendaoud, A. EL-Abidi, H. Amiry, M. Benhmida, S. Bounouar, B. Zohal, H. Boussetta, A. Zrhaiba, A. Elhassnaoui, Evolution of the physical parameters of photovoltaic generators as a function of temperature and irradiance: new method of prediction based on the manufacturer's datasheet, *Energy Convers. Manag.* 203 (2020), <https://doi.org/10.1016/j.enconman.2019.112141>.
- [30] T. Nguyen-Duc, H. Nguyen-Duc, T. Le-Viet, H. Takano, Single-diode models of PV modules: a comparison of conventional approaches and proposal of a novel model, *Energies* 13 (2020), <https://doi.org/10.3390/en13061296>.
- [31] A.M. Humada, S.Y. Darweesh, K.G. Mohammed, M. Kamil, S.F. Mohammed, N. K. Kasim, T.A. Tahseen, O.I. Awad, S. Mekhilef, Modeling of PV system and parameter extraction based on experimental data: review and investigation, *Sol. Energy* 199 (2020) 742–760, <https://doi.org/10.1016/j.solener.2020.02.068>.
- [32] E. Roibás-Millán, D. Alfonso-Corcuera, J. Cubas, J.M. Alvarez, S. Pindado, A. M. Gomez-Sanjuan, Performance analysis of photovoltaic systems: research at IDR/UPM Institute, in: 20TH IEEE Int. Conf. Environ. Electr. Eng. - IEEE EEEIC 2020, Institute of Electrical and Electronics Engineers, IEEE, Madrid, Spain, 2020, pp. 769–774, <https://doi.org/10.1109/IEEEIC/ICPSEurope49358.2020.9160719>.
- [33] E. Roibás-Millán, J.L. Cubero-Estalrich, A. Gonzalez-Estrada, R. Jado-Puente, M. Sanabria-Pinzón, D. Alfonso-Corcuera, J.M. Alvarez, J. Cubas, S. Pindado, Lambert W-function simplified expressions for photovoltaic current-voltage

- modelling, in: 20TH IEEE Int. Conf. Environ. Electr. Eng. - IEEE EEEIC 2020, Institute of Electrical and Electronics Engineers, IEEE, Madrid, Spain, 2020, pp. 1630–1635, <https://doi.org/10.1109/EEEIC49358.2020.9160734>.
- [34] T. Easwarakhanthan, J. Bottin, I. Bouhouch, C. Boutrit, Nonlinear minimization algorithm for determining the solar cell parameters with microcomputers, *Int. J. Sol. Energy* 4 (1986) 1–12, <https://doi.org/10.1080/01425918608909835>.
- [35] S. Pindado, J.L. Cubero-Estalrich, A. Gonzalez-Estrada, R. Jado-Puente, M. Sanabria-Pinzón, D. Alfonso-Corcuera, J.M. Alvarez, E. Roibás-Millán, J. Cubas, *Simplified Approaches to Solar Cell/panel Equivalent Circuit Modelling Based on the Lambert W-function*, 2020.
- [36] A. Bellini, S. Bifaretti, V. Iacovone, C. Cornaro, Simplified model of a photovoltaic module, *Appl. Electron.* (2009) 47–51. [http://ieeexplore.ieee.org/xpls/abs\\_all.jsp?arnumber=5289294](http://ieeexplore.ieee.org/xpls/abs_all.jsp?arnumber=5289294).
- [37] M.U. Siddiqui, A.F.M. Arif, A.M. Bilton, S. Dubowsky, M. Elshafei, An improved electric circuit model for photovoltaic modules based on sensitivity analysis, *Sol. Energy* 90 (2013) 29–42, <https://doi.org/10.1016/j.solener.2012.12.021>.
- [38] H. Ibrahim, N. Anani, Variations of PV module parameters with irradiance and temperature, *Energy Procedia* 134 (2017) 276–285, <https://doi.org/10.1016/j.egypro.2017.09.617>.
- [39] S. Yadir, R. Bendaoud, A. EL-Abidi, H. Amiry, M. Benhmida, S. Bounouar, B. Zohal, H. Boussetta, A. Zrhaiba, A. Elhassnaoui, Evolution of the physical parameters of photovoltaic generators as a function of temperature and irradiance: new method of prediction based on the manufacturer's datasheet, *Energy Convers. Manag.* 203 (2020) 112141, <https://doi.org/10.1016/j.enconman.2019.112141>.
- [40] S. Lineykin, Five-parameter model of photovoltaic cell based on STC data and dimensionless, *Electr. Eng. Electron.* (2012) 1–5.
- [41] M.G. Villalva, J.R. Gazoli, E.R. Filho, Comprehensive approach to modeling and simulation of photovoltaic arrays, *IEEE Trans. Power Electron.* 24 (2009) 1198–1208, <https://doi.org/10.1109/TPEL.2009.2013862>.
- [42] L. Peng, Y. Sun, Z. Meng, Y. Wang, Y. Xu, A new method for determining the characteristics of solar cells, *J. Power Sources* 227 (2013) 131–136, <https://doi.org/10.1016/j.jpowsour.2012.07.061>.
- [43] S. Oprea, C. Radoi, A. Florescu, A.S. Savu, A.I. Lita, Power architectures and power conditioning unit for very small satellites, B. N., M.T. N., B. F., K. E. (Eds.), in: *Energy Harvest. Energy Effic. Lect. Notes Energy*, vol. 37 Springer, Cham, 2017, pp. 491–539, [https://doi.org/10.1007/978-3-319-49875-1\\_17](https://doi.org/10.1007/978-3-319-49875-1_17).
- [44] A. Aoudeche, X. Zhao, K.D. Kerrouche, Design of a high performance electrical power system for an earth observation nano-satellite, in: *Proc. 2018 Int. Conf. Electron. Electr. Eng. Technol.*, 2018, pp. 140–146, <https://doi.org/10.1145/3277453.3286093>.
- [45] A. Ali, M.R. Mughal, H. Ali, L. Reyneri, Innovative power management, attitude determination and control tile for CubeSat standard NanoSatellites, *Acta Astronaut.* 96 (2014) 116–127, <https://doi.org/10.1016/j.actaastro.2013.11.013>.
- [46] A. Aldaw, M. Abaker, A. Babiker, A. Alnabi, Analysis of cube-sat electrical power system Architecture, *Sci. Technol. Innov. J.* 1 (2017) 1–6.
- [47] J. Li, M.S. Mazzola, Accurate battery pack modeling for automotive applications, *J. Power Sources* 237 (2013) 215–228, <https://doi.org/10.1016/j.jpowsour.2013.03.009>.
- [48] S.M. Mousavi, M. Nikdel, Various battery models for various simulation studies and applications, *Renew. Sustain. Energy Rev.* 32 (2014) 477–485, <https://doi.org/10.1016/j.rser.2014.01.048>.
- [49] A. Fotouhi, D.J. Auger, K. Propp, S. Longo, M. Wild, A review on electric vehicle battery modelling: from Lithium-ion toward Lithium-Sulphur, *Renew. Sustain. Energy Rev.* 56 (2016) 1008–1021, <https://doi.org/10.1016/j.rser.2015.12.009>.
- [50] H. Kang, M. Rim, *Samsung INR18650-29E Lithium-Ion Rechargeable Cell, Specifications of product*, 2012.
- [51] S. Chen, A. Saber, T. Khandelwal, General battery modeling and simulation using non-linear open circuit voltage in power system analysis, in: *IEEE Power Energy Soc. Gen. Meet.*, IEEE, 2016, <https://doi.org/10.1109/PESGM.2016.7741929>.
- [52] T.R.B. Grandjean, A. McGordon, P.A. Jennings, Structural identifiability of equivalent circuit models for li-ion batteries, *Energies* 10 (2017), <https://doi.org/10.3390/en10010090>.
- [53] V. Sangwan, A. Sharma, R. Kumar, A.K. Rathore, Equivalent circuit model parameters estimation of Li-ion battery: C-rate, SOC and Temperature effects, in: *IEEE Int. Conf. Power Electron. Drives Energy Syst. PEDES 2016*, IEEE, 2017, <https://doi.org/10.1109/PEDES.2016.7914369>.
- [54] F. Vigier, A.-F. Castric, F. Pathe, SAFT Batteries. *VES16 User's Handbook*. Ref.: R0113-11, 2012. Edition/Issue : 1. March 28th, 2012.